Influence of Component Errors of Rotary Axes on a Machining Test of Cone Frustum by Five-axis Machine Tools

Cefu Hong[1], Soichi Ibaraki[1,#] and Atsushi Matsubara[1]

1 Department of Micro Engineering, Graduate School of Engineering, Kyoto University, Yoshida-honmachi, Sakyo-ku, Kyoto 606-8501, Japan
Corresponding Author / E-mail: ibaraki@prec.kyoto-u.ac.jp, TEL: +81-75-753-5227, FAX: +81-75-753-5227

KEYWORDS : five-axis machine tool, machining test, cone frustum, location error, component error

A machining test of cone frustum, described in NAS (National Aerospace Standard) 979, is widely accepted by machine tool builders to evaluate the machining performance of five-axis machine tools. This paper discusses the influence of various error causes associated with rotary axes on a five-axis machine tool on the machining geometric accuracy of the cone frustum machined by this test. Location errors, or kinematic errors, associated with rotary axes, such as the squareness error of a rotary axis and a linear axis, can be seen as the most fundamental errors in five-axis kinematics. Other more complex errors, such as the deformation caused by the gravity, the run-out of a rotary axis, the angular positioning error of a rotary axis, can be modeled as component errors of a rotary axis. This paper shows that some error factors, such as run-out and angular motion of C-axis, impose sufficiently small effect on circularity error on the cone frustum machining test. It also clarifies that a center shift of a C-axis caused by the B-axis rotation can be a potentially critical error factor for cone frustum machining test.

Manuscript received: July 15, 2009 / Accepted: August 15, 2009

1. Introduction

Five-axis machine tool is extensively used in sculptured surface machining with the advantages including higher metal removal rate, significantly shorter cutting time and improved surface finish[1]. With recent rapid acceptance of five-axis machine tools in the manufacturing market, there are more cases where it is used in machining applications requiring higher machining accuracy, such as die and mold manufacturing. However, accompanying with accumulation of errors due to the increased number of synchronous motion axes, the overall motion accuracy of a five-axis machine tool is often significantly worse than that of a conventional three-axis machine tool. To improve its motion accuracy, it is crucial to develop its accurate and efficient measurement methodology for its accuracy inspection.

NAS 979[2] describes the evaluation of machining accuracy of a five-axis machine tool by the machining of a cone frustum which is widely accepted to many machine tool builders as a final performance test for five-axis machine tools. Equivalent non-cutting measurement methods using a ball bar measurement have been also studied by Ihara et al. [3].

Kinematic errors are the most fundamental error factors in the five-axis kinematics. ISO10791-1~3 describes measurement schemes to identify kinematic errors. Many researches in the literature[1,4] have also studied ball bar measurements to identify kinematic errors. However, from our experiences, on the latest small-sized five-axis machine tools, the circularity error of the machined workpiece in cone frustum machining tests can be typically as small as five to ten micrometers. In such a case, the influence of the machine's kinematic errors is generally quite small, which suggests that more complex error factors, such as the gravity deformation, angular positioning error of a rotary axis, run-out or "angular motion" of a rotary axis, are potentially dominant error factors in cone frustum machining tests. Such more complex error factors are collectively called component errors in this paper. With simulating and analyzing the influence of component errors, the objective of this paper is to clarify critical error factors on the machining test of cone frustum by five-axis machine tools. Experimental case study is conducted for the verification.

2. Definition and Modeling of Location and Component errors

This paper considers a five-axis machine tool with a tilting rotary table, as is shown in Fig. 1. Kinematic errors of rotary axes are shown in Table 1[5]. For example, as is shown in Fig. 2 (a), kinematic errors δx_{CB} and δy_{CB} , which are defined as position errors of rotation center of C-axis with respect to B-axis in X and Y directions, do not change according to rotation of C-axis. As is shown in Fig. 2 (b), the run-out of C-axis can not be described as kinematic errors δx_{CB} and δy_{CB}. However, it could be modeled as position errors of rotation center of C-axis in X and Y directions, which change according to the rotation of C-axis ($\delta x_{CB}(C)$ and $\delta y_{CB}(C)$). Also, so-called "angular motion", which is shown in Fig. 2 (c), can be modeled as angular errors

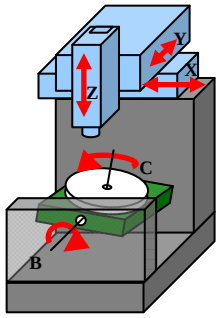

Fig. 1 Five-axis machine tool with a tilting rotary table

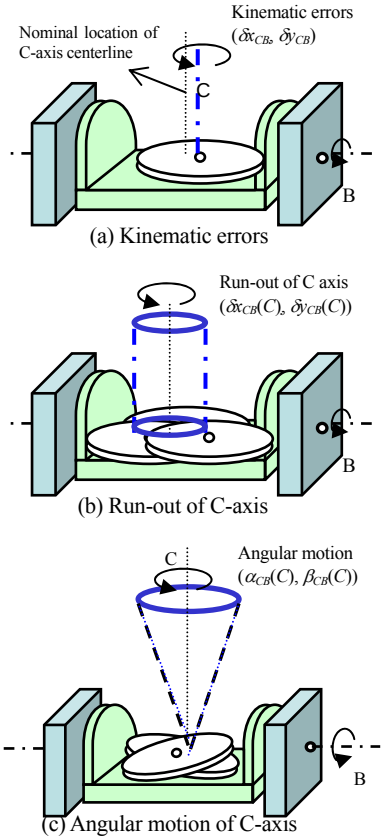

Fig. 2 Examples of location and component errors

changed according to rotation of C-axis ($\alpha_{CB}(C)$ and $\beta_{CB}(C)$).

As is shown in Table 2, most motion errors of rotary axes on five-axis machine tool can be modeled as kinematic errors that change according to rotation of rotary axes, which correspond to the term "component errors" defined in ISO230-7[6]. Note that kinematic errors correspond to the term "location errors" in ISO230-7.

The influence of each location error on the displacement of a tool relative to a workpiece can be simulated by using the kinematic model of five-axis configuration. This model is well known in the literature[1] and omitted in this paper. The influence of each component error on the machining error can be analogously simulated by simply extending this model.

3. Setup of cone frustum machining test

Figure 3 shows machining configuration and parameters of tilted cone frustum to be considered in this paper. For simplicity of computation, this paper simulates a tool center location trajectory which can be interpreted as a geometric error profile of the machined workpiece when the tool radius is zero. D, φ, ψ are defined as diameter of tool path, tilted angle of cone frustum about Y-axis in the workpiece coordinate system and half-apex angle of the cone frustum, respectively. The workpiece coordinate system is attached to the rotary table. Its XY origin is defined at the rotation center of C-axis,

Table 1 Descriptions of location errors associated with rotary axes

Symbol	Description
α_{BY}	Squareness of B to Z axis
β_{BY}	Orientation of B axis around Y axis
γ_{BY}	Squareness of B to X axis
α_{CB}	Squareness of C to B axis
δx_{BY}	Linear shift of B axis in X direction
δy_{BY}	Linear shift of B axis in Y direction
δz_{BY}	Linear shift of B axis in Z direction
δx_{CB}	Linear shift of C axis in X direction

Table 2 Descriptions of component errors associated with rotary axis

Symbol	Description
$\alpha_{BY}(B)$	Orientation changes of B-axis with B rotation
$\beta_{BY}(B)$	Angular error of B-axis rotation
$\gamma_{BY}(B)$	Orientation changes of B-axis with B rotation
$\alpha_{CB}(C, B)$	Orientation changes of C-axis with C, B rotation
$\beta_{CB}(C, B)$	Orientation changes of C-axis with C, B rotation
$\gamma_{CB}(C, B)$	Angular error of C-axis rotation
$\delta x_{BY}(B)$	Location changes of B-axis center with B rotation
$\delta y_{BY}(B)$	Location changes of B-axis center with B rotation
$\delta z_{BY}(B)$	Location changes of B-axis center with B rotation
$\delta x_{CB}(C, B)$	Location changes of C-axis center with C, B rotation
$\delta y_{CB}(C, B)$	Location changes of C-axis center with C, B rotation
$\delta z_{CB}(C, B)$	Location changes of C-axis center with C, B rotation

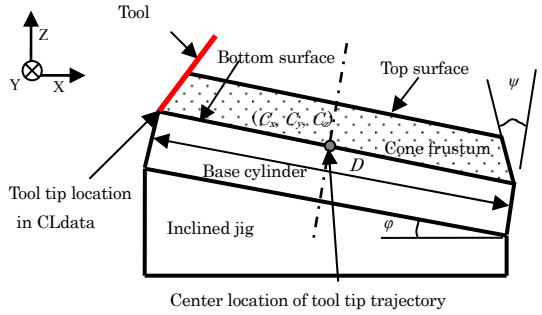

Fig. 3 Setup for machining of cone frustum

Table 3 Simulation conditions for the machining test of cone frustum

Parameter	Value
Diameter of tool path, D (mm)	129.9
Tilt angle, φ(°)	15
Half-apex angle, ψ (°)	30
Center location of tool path (C_x, C_y, C_z) (mm)	(-81.8, 0,189.3)
Feedrate (mm/min)	1,000

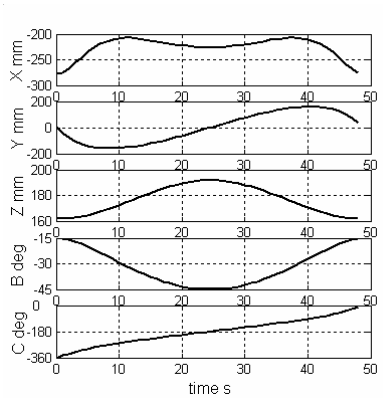

Fig. 4 Command trajectory of each axis (assuming feedrate 1000 mm/min)

while its Z origin is defined at the rotation center of B-axis. (C_x, C_y, C_z) is the center location of tool tip trajectory in the workpiece coordinate system.

Table 3 shows the conditions for cone frustum machining test used in simulations presented in Section 4. The command trajectory

of each axis under this condition is shown in Fig. 4.

Clearly, command trajectories are dependent on machining conditions shown in Table 3, and thus simulation results to be presented in Section 4 may significantly vary as well. It should be, however, noted that Ihara and Tanaka[3] showed that command trajectories for cone frustum machining can be categorized into two groups. When $\varphi<\psi$, C-axis rotates for 360°, while B-axis rotates in a smaller range, as is shown in Fig. 4. However when $\varphi>\psi$, B-axis rotates in a larger range, while C-axis does not rotate for 360°.

The following section only shows simulation results for the case $\varphi<\psi$(φ=15°, ψ=30°). Although the influence of each error source may significantly vary quantitatively, it can be said that its qualitative influence is similar to some extent for any conditions with $\varphi<\psi$. Although simulation results for the case $\varphi>\psi$ are not presented due to the paper length limitation, the same analysis could be conducted.

4. Influence of component errors

Previous studies in the literature[7] has discussed the influence of location errors (kinematic errors) on the machining geometric error in a cone frustum machining test. The objective of this paper is to further extend this analysis to more complex component errors of a rotary axis. The analysis on the influence of location errors is omitted in this paper due to the limitation in paper length. This paper considers the following component errors of rotary axes, which are potentially common errors observed in commercial five-axis machine tools.

4.1 Influence of axial position error and angular positioning error of B- and C-axis

The axial position error of C-axis is simulated as follows:

$$\begin{cases} \delta x_{CB}(C_i) = M + (N-M)\dfrac{C_i+360}{C'+360} & (C_i = -360^\circ \rightarrow C') \\ \delta x_{CB}(C_i) = M + (N-M)\dfrac{C_i}{C'} & (C_i = C' \rightarrow 0^\circ) \end{cases} \quad (1)$$

where M, N and C' are given by:

M=N(0 μm, 2 μm), N=N(0 μm, 2 μm), C' = N(-180°, 180°),

where $N(\mu, \sigma)$ represents a normally distributed random number with the mean value μ and the standard deviation σ. C_i is the command angular position of C-axis in degree. Note that Eq. (1) represents a axial direction position error proportional to C angular position, with a different gradient before and after C', such that it becomes continuous at C=0°. Such an error is typically caused by the geometric inaccuracy of a bearing lace.

Table 4 Influence of axial position error, angular positioning error and gravity deformation on B-axis on circularity

Contributor	Circularity error (1 σ) (μm)
Axial position error of B-axis	0.8
Axial position error of C-axis	0.6
Angular positioning error of B-axis	1.1
Angular positioning error of C-axis	1.4
Gravity deformation on B-axis	<0.1

Assuming the axial position error of C-axis modeled in Eq. (1), the geometric error profile of the machined cone frustum workpiece is simulated by using the simulation model analogous to the one presented in [1]. The circularity error, defined as the difference between maximum and minimum radial errors, is computed from the simulated error trajectory. Note that the center of simulated error trajectory is set to the point where the smallest circularity error is obtained. Same simulations are repeated for 10000 times with randomly given M, N and C', and the standard deviation (1 σ) of simulated circularity errors is calculated as is shown in Table 4. The influence of the axial position error of B-axis is simulated in the same way with Eq. (1).

Furthermore, angular positioning error of B- and C-axis, $\beta_{BY}(B_i)$ and $\gamma_{CB}(C_i)$ are simulated in the same way as is shown in Eq. (1), while M and N are given by M = N(0°, 0.002°), N = N(0°, 0.002°). The simulation results are shown in Table 4.

Compared to the standard deviation of each given error, its influence on the circularity error is relatively small. For example, for axial position error of B and C axes, the standard deviation of circularity error is less than half of that of given errors.

4.2 Influence of gravity deformation on B-axis

One of errors caused by gravity deformation is displacement of B-axis in Z direction, which is simulated as follows:

$$\begin{cases} \delta z_{BY}(B_i) = M + (N-M)\dfrac{B_i+90}{90} & (B_i = -90^\circ \rightarrow 0^\circ) \\ \delta z_{BY}(B_i) = N + (M-N)\dfrac{B_i}{90} & (B_i = 0^\circ \rightarrow 90^\circ) \end{cases} \quad (2)$$

where M and N are given by:

M=N(0 μm, 2 μm), N=N(0 μm, 2 μm),

B_i is the command angular position of B-axis in degree.

As is shown in Table 4, the simulation result shows that the standard deviation (1 σ) of circularity error is smaller than 0.1 μm. It suggests that gravity deformation on B-axis in Z direction has a negligibly small influence on circularity of cone frustum.

4.3 Influence of run-out and angular motion of B- and C-axis

Figure 2 shows run-out and angular motion of C-axis. Run-out and angular motion of C-axis considered in this simulation are shown as follows:

$$\begin{cases} \delta x_{CB}(C_i) = a_1 \cos(C_i + \zeta) \\ \delta y_{CB}(C_i) = a_1 \sin(C_i + \zeta) \end{cases} \quad (3)$$

$$\begin{cases} \alpha_{CB}(C_i) = a_2 \cos(C_i + \zeta) \\ \beta_{CB}(C_i) = a_2 \sin(C_i + \zeta) \end{cases} \quad (4)$$

where a_1, a_2 and ζ are given by:

a_1=N(0 μm, 2 μm), a_2=N(0°, 0.002°), ζ= N(0°, 180°).

Table 5 Influence of run-out and angular motion on circularity

Contributor	Circularity error (1 σ) (μm)
Run-out of B axis	0.3
Run-out of C axis	<0.1
Angular motion of B axis	1.1
Angular motion of C axis	<0.1

The run-out and angular motion of B-axis is modeled in the same way as C-axis. The simulation results are shown in Table 5. From the simulation results, the influence of run-out and angular motion of C-axis on circularity is sufficiently small compared to given errors.

4.4 Influence of change in the position or orientation of rotation centerline with B and C rotation

The change in the position or orientation of rotation centerline caused by axis rotation from nominal centerline is considered in this simulation. The modeling of the simulation are shown as follows:

$$\begin{cases} \delta x_{CB}(C_i) = b_1 \dfrac{C_i+360}{C'+360}\cos(\zeta) \\ \delta y_{CB}(C_i) = b_1 \dfrac{C_i+360}{C'+360}\sin(\zeta) \end{cases} (C_i = -360^\circ \rightarrow C') \quad (5)$$

$$\begin{cases} \delta x_{CB}(C_i) = b_1 \dfrac{C_i}{C'}\cos(\zeta) \\ \delta y_{CB}(C_i) = b_1 \dfrac{C_i}{C'}\sin(\zeta) \end{cases} (C_i = C' \rightarrow 0^\circ) \quad (6)$$

where b_1, C' and ζ are given by:

b_1=N(0 μm, 2 μm), C' = N(-180°, 180°), ζ= N(0°, 180°).

The simulation results are shown in Table 6. Compared with previous simulation, change in the position or orientation of rotation centerline of C axis from nominal centerline affects more the circularity of cone frustum. On the other hand, the change in the position or orientation of rotation center line of B-axis has a sufficiently small influence on circularity of cone frustum, compared to given errors.

Table 6 Influence of change in the position or orientation of rotation centerline of B- and C-axis with axis rotation on circularity

Contributor	Circularity error (1σ) (μm)
Change in the position of rotation centerline of B axis with B rotation	0.1
Change in the position of rotation centerline of C axis with C rotation	0.9
Change in the orientation of rotation centerline of B axis with B rotation	0.2
Change in the orientation of rotation centerline of C axis with C rotation	2.8

4.5 Influence of run-out and angular motion of C-axis changed by B-axis rotation

The simulation result conducted in Section 4.3 shows that run-out and angular motion of C-axis has negligibly small influence on circularity. This section considers the case where the run-out or angular motion of C-axis increased as B rotates from 0°. This error, caused mainly by the gravity-induced deformation, is often the case in practice. Run-out of C-axis changed by B-axis rotation is shown as follows:

$$\begin{cases} \delta x_{CB}(C_i, B_i) = a_1 \cos(C_i + \zeta)\left(\frac{1}{2} + \left|\frac{B_i}{45^\circ}\right|\right) \\ \delta y_{CB}(C_i, B_i) = a_1 \sin(C_i + \zeta)\left(\frac{1}{2} + \left|\frac{B_i}{45^\circ}\right|\right) \end{cases} \quad (7)$$

where a_1 and ζ are given by:

$$a_1 = N(0\ \mu m, 2\ \mu m),\ \zeta = N(0^\circ, 180^\circ),$$

B_i and C_i are the command angular position of B- and C-axis in degree, respectively.

Table 7 Influence of run-out and angular motion of C-axis changed by B-axis rotation on circularity

Contributor	Circularity error (1σ) (μm)
Run-out of C-axis caused by B- and C-axis rotation	0.8
Angular motion of C-axis caused by B- and C-axis rotation	2.4

Angular motion of C-axis changed by B-axis rotation is simulated in the same way as Eq. (7) shows, while a_1 is given by $N(0°, 0.002°)$. The simulation results are shown in Table 7. Compared with Section 4.3, circularity of cone frustum is more sensitive to run-out and angular motion of C-axis changed by B-axis rotation.

From the analysis mentioned above, some component errors such as displacement of B-axis caused by gravity deformation in Z direction and run-out and angular motion of C-axis have a negligibly small influence on circularity of cone frustum. However, change in the position or orientation of C-axis rotation centerline from nominal centerline with B and C rotation, run-out and angular motion of C-axis changed by B-axis rotation could be critical factors for cone frustum machining test.

It has been shown in [7] that a center offset of a rotary axis, one of kinematic errors, has a significant influence on the circularity error of machined workpiece. In typical machine setup by an operator, for example, the location of C-axis rotation center is measured with B=0°. It is possible that the C-axis rotation center is moved as the B-axis rotates from B=0°. Its possible causes include the gravity influence. The simulation presented in Section 4.4 shows that such an error may cause a large circularity error, even if the center offset of C-axis is sufficiently small when B=0°. Analogous observation can be made for the run-out or the angular motion of C-axis.

5. Experimental case study

The analysis in previous sections suggests that a center shift of a C- axis caused by the B-axis rotation can be a potentially critical error factor for cone frustum machining test. This section presents the experimental validation for the discussion presented in previous sections. It also suggests a practical methodology to diagnose a major cause of machining geometric errors in cone frustum machining test.

Table 8 Identified kinematic errors associated with rotary axes

Kinematic error	Identified value
α_{BY}(°)	0.0005
β_{BY}(°)	0.0001
γ_{BY}(°)	0.0001
α_{CB}(°)	-0.0006
δx_{BY}(μm)	-
δy_{BY}(μm)	-
δz_{BY}(μm)	-
δx_{CB}(μm)	2.1

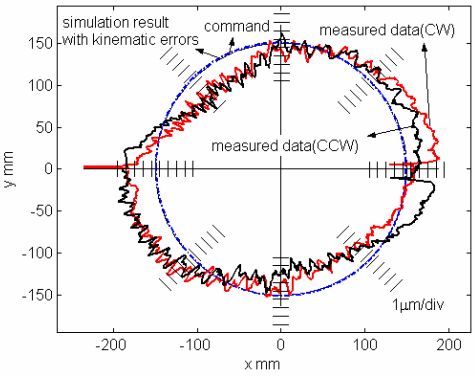

(a) Influence of kinematic errors

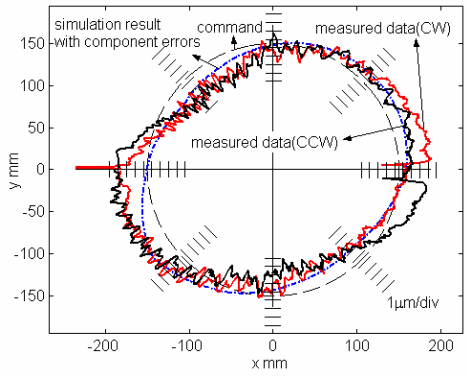

(b) Influence of center shift of C axis

Fig. 5 Contour error profiles for the cone frustum CL trajectory measured by ball bar measurement

Instead of actual machining test, a contouring error profile was measured with the same CL (cutter location) trajectory as in a cone frustum machining test by a ball bar measurement [3]. Test conditions are summarized in Table 3, and the ball bar nominal length is 150 mm. To first investigate the influence of kinematic errors, eight kinematic errors shown in Table 1 were experimentally identified by using a set of ball bar measurements presented in [4]. The identified kinematic errors are shown in Table 8. Since the rotation center of rotary axes were carefully identified before a cone frustum measurment, δx_{BY}, δy_{BY}, δz_{BY} are assumed to be zero in the following simulation.

Fig. 5 shows contour error profiles for the cone frustum CL trajectory measured by ball bar measurement. The circularity error is 12.4 μm for clockwise (CW) rotation, and 9.2 μm for counter-clockwise (CCW) rotation. Fig. 5 (a) also shows a simulated error trajectory to show the influence of identified kinematic errors. It can be observed that the influence of kinematic errors shown in Table 8 is quite small; the circularity error of the simulated error trajectory is only 0.3 μm.

To further investigate major error causes, the motion accuracy of C-axis rotation was measured for different B-axis positions. Fig. 6 illustrates its measurement scheme. A reference ball of sufficiently high geometric accuracy is attached to the machine's spindle. A displacement sensor is installed on a rotary table, pointing in the X-

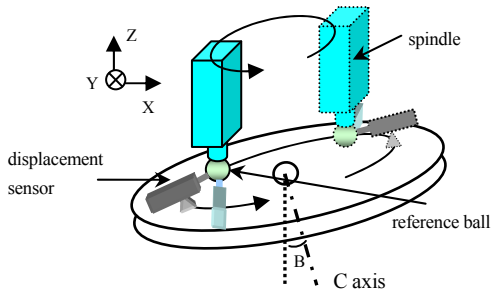

Fig. 6 Scheme for measuring motion accuracy of C-axis by displacement sensor

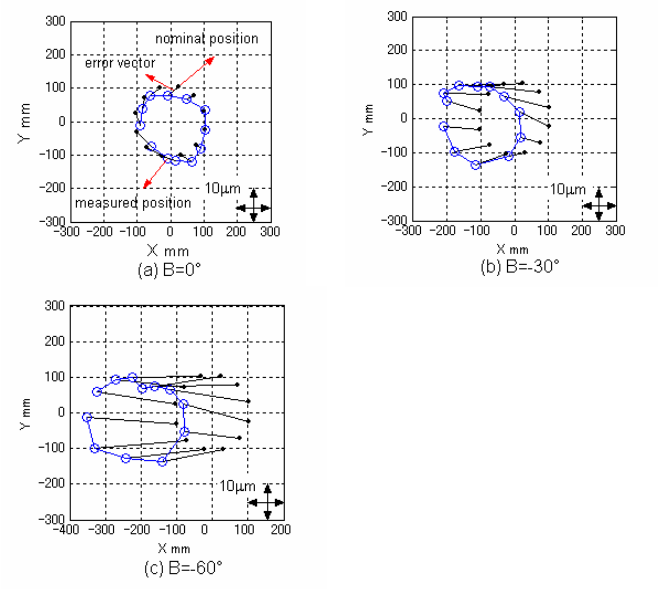

Fig. 7 Motion error profile of C axis in B-axis

direction (of the workpiece coordinates) as shown in Fig. 6. As the rotary table is indexed by C-axis, linear axes are synchronously driven such that the reference ball follows the sensor. For every 30 degree of C-axis rotation, the displacement of the ball is measured. The same measurement is repeated with the sensor pointing in the Y-direction. Notice that since the sensor is installed on the table, measured displacements constitute error vectors in the workpiece coordinate system. By converting them into vectors in the global coordinate system, and magnifying them by a factor of 10,000, Fig. 7 (a)-(c) shows measured position errors of the ball with the C-axis rotation, in the coordinate system attached to the B-axis. The same measurement was repeated for B=0°, -30°, and -60°. Note that in the CL trajectory shown in Fig.4, the B-axis varies from -15° to -45°.

From Fig. 7 (a), it can be observed that the error is sufficiently small at B=0°. In Fig. 7 (b) and (c), the center of the error trajectory is significantly shifted to –X direction. This is mostly due to the miscalibration of the B-axis rotation center in the Z-direction, i.e. δz_{BY}. In addition, it can be observed that the radius of the error trajectory becomes larger as the B-angle increases. This suggests that the run-out, or angular motion, of C-axis gets larger as the B-angle increases, which is likely caused by the gravity-induced deformation. Furthermore, even when δz_{BY} is compensated for, a shift of the rotation center of C-axis is observed, which is also considered to be caused by the gravity-induced deformation.

The influence of such an error on the contour error in the cone frustum CL trajectory is then simulated. After removing the influence of kinematic errors, the C-axis position error shown in Fig. 7 (a)-(c) is stored in a look-up table for each combination of B- and C-axis positions. For the given cone frustum CL trajectory, the C-axis error profile is calculated by interpolating this look-up table. Fig. 5 (b) shows the simulated contour error profile. Measured profiles are the same as those in Fig. 5 (a). The simulated trajectory matches well with the measured trajectory, which indicates that the C-axis error presented in Fig. 7 (a)-(c) is a major cause of contour error in cone frustum machining.

6. Conclusions

An analysis method is proposed for clarifying the influence of error causes, especially component errors of a rotary axis, on circularity of cone frustum by the machining test of cone frustum. The analysis suggests that a center shift of C-axis caused by axis rotation can be a potentially critical error factor for cone frustum machining test. Experiments have verified that a center shift of a C-axis caused by the B-axis rotation, is a primal cause for circularity error on a cone frustum machining test.

REFERENCES

1. M. Sharif Uddin, Soichi Ibaraki, Atsushi Matsubara, Tetsuya Matsushita, "Prediction and compensation of machining geometric errors of five-axis machining centers with kinematic errors", Precision Engineering, Vol.33, No.2, pp.194-201, 2009.

2. NAS979, "Uniform Cutting Test – NAS Series", Metal Cutting Equipments, 1969.

3. Yukitoshi Ihara, Kazuya Tanaka, "Ball Bar Measurement Equivalent to Cone Frustum Cutting on Multi-axis Machine: Comparison of Ball Bar Measurement with Cutting Test on Spindle-tilt Type 5-axis MC"(in Japanese), Journal of the Japan Society of Precision Engineering, Vol.71, No.12 pp.1553-1557, 2005.

4. Akinori Saito, Masaomi Tsutsumi, Kentaro Ushiku, "Development of Calibration Methods of 5-axis Controlled Machining Centers (2nd Report): Estimation of Positional and Angular Deviation by Means of Simultaneous 3-axis Motion"(in Japanese), Journal of the Japan Society of Precision Engineering, Vol.69, No.2, pp.268-273, 2003.

5. Akinori Saito, Masaomi Tsutsumi, Shigetata Mikami, Souvannavong Sisavath, "Development of Calibration Methods of 5-axis Controlled Machining Centers (3rd Report): Measurement Methods for Various Structural Configurations of 5-axis Controlled Machining Centers "(in Japanese), Journal of the Japan Society of Precision Engineering, Vol.69, No.6, pp.809-814, 2003.

6. ISO230-7, "Test Code for Machine Tools – Part 7: Geometric Accuracy of Axes of Rotation", 2006.

7. Tetsuya Matsushita, Tadahiro Oki, Atsushi Matsubara, "The Accuracy of Cone Frustum Machined by Five-axis Machine Tool with Tilting Table"(in Japanese), Journal of the Japan Society of Precision Engineering, Vol. 74, No. 6, pp. 632-636, 2008.